2016

Upper Extremity Inverse Dynamics Model for Loftstrand Crutch-Assisted Gait in Children with Osteogenesis Imperfecta

Brooke A. Slavens
Marquette University, brooke.slavens@marquette.edu

Neha Bhagchandani
Marquette University

Mei Wang
Marquette University, mei.wang@marquette.edu

Peter A. Smith
Shriners Hospitals for Children

Gerald F. Harris
Marquette University, gerald.harris@marquette.edu

20 UPPER EXTREMITY INVERSE DYNAMICS MODEL FOR LOFSTRAND CRUTCH- ASSISTED GAIT IN CHILDREN WITH OSTEOGENESIS IMPERFECTA

Brooke A. Slavens, Ph.D.[1-4]
Neha Bhagchandani, M.S.[4]
Mei Wang, Ph.D.[4]
Peter A. Smith, M.D.[3]
Gerald F. Harris, Ph.D., P.E.[3,4]

[1] Department of Occupational Science & Technology, University of Wisconsin-Milwaukee, Milwaukee, WI
[2] Rehabilitation Research Design and Disability (R_2D_2) Center, University of Wisconsin-Milwaukee, Milwaukee, WI
[3] Shriners Hospitals for Children, Chicago, IL
[4] Orthopaedic and Rehabilitation Engineering Center (OREC), Marquette University and The Medical College of Wisconsin, Milwaukee, WI

INTRODUCTION

Our aim is to quantify upper extremity (UE) forces and moments during Lofstrand crutch-assisted gait to better predict skeletal loading during ambulatory and functional activities in children with osteogenesis imperfecta (OI). Approximately 566,000 crutch users live in the United States, of which among these are a population of children with OI.[1] Due to long-term assistive device usage, these children may be at an increased risk for developing UE pathologies. Literature has shown that longer-term crutch users experience altered UE joint loads, and may be at risk for development of musculoskeletal injury, early onset osteoarthritis, and carpal tunnel syndrome. Previous studies evaluating UE dynamics during assisted gait are limited. Our goal is to develop a three-dimensional (3-D) UE biomechanical model to quantify joint dynamics during Lofstrand crutch-assisted gait in children with OI. Our work recognizes that a pediatric biomechanical model may be a valuable tool for clinicians to characterize and better understand UE dynamics of crutch-assisted gait in children with OI.[2] While motion

analysis has been extensively used to study gait, limited work has been conducted to characterize UE dynamics during Lofstrand crutch-assisted gait.[3,4] Motion analysis is a noninvasive technique that allows evaluation of multi-planar motion during functional activities.[5,6] Improved motion analysis technology and modeling software has allowed more rapid development of complex biomechanical models, such as those needed to study UE kinematics and kinetics.

OI, a genetic disorder characterized by fragile bones, is a pediatric pathology associated with Lofstrand crutch use. It is caused by mutation in genes that affects the body's production of the collagen found in bones and other tissues.[7] In addition to fractures, people with OI often have muscle weakness, hearing loss, fatigue, joint laxity, curved bones, scoliosis, blue sclerae, dentinogenesis imperfecta (brittle teeth), and short stature.[8] OI has a prevalence of 1/5,000 to 1/10,000, with an estimated 20,000 to 50,000 cases in the U.S.[6,9] OI is divided into eight types (I, II, III, IV, V, VI, VII and VIII) based on clinical, radiographic and genetic characteristics.

OI type I is the mildest form of OI, and is also the most common type in this population. These children suffer from mild fractures and have frequent shoulder and elbow dislocations.[8] Children with OI type I commonly use assistive devices, such as Lofstrand crutches, for community ambulation (Figure 1). Those using Lofstrand crutches present a possibility of recurrent fractures due to repetitive, high forces placed on the UEs. These long-term crutch users may be at an increased risk for the development of UE joint pain and pathology.

Klimaitis and colleagues, as early as 1988, found that bearing weight through the upper limbs may hasten the development of degenerative arthritis in the shoulder, possibly by contributing to mechanical disruption of the rotator cuff.[10] In addition, multiple authors have reported that superiorly directed weight-bearing forces may potentially threaten glenohumeral joint integrity, as translation of the humeral head and subsequent impingement of subacromial structures may occur if these forces are not matched by an appropriate response of the rotator cuff and thoracohumeral depressor musculature.[11,12] The literature shows that long-term assistive device usage may result in upper limb pathologies, such as destructive shoulder arthropathy and degenerative arthritis of the shoulder.[13,14]

Figure 1. Patient with osteogenesis imperfecta (OI) using Lofstand crutches. She is instrumented with the UE marker system and is using the kinetic Lofstrand crutches.

With regard to more distal joints, an association between the development of carpal tunnel syndrome and the use of assistive devices has also been reported.[15-17] Repetitive impulse loading with prolonged wrist extension and with radial deviation have been identified as proposed risk factors for pathology.[16,17]

The inverse dynamics of Lofstrand crutch-assisted gait in the pediatric population has been reported only to a small extent.[3,4] Unlike lower extremity motion, UE motion does not follow a repeating pattern, thus making it difficult to standardize and compare data among different studies. The International Society of Biomechanics (ISB) has recently established

recommendations for modeling UE joint coordinate systems.[18] With this effort, communication among researchers and physicians has been enhanced through these modeling standards.

New efforts are underway to utilize instrumented Lofstrand crutches for characterization of UE dynamics during gait in children with OI. Tri-axial forces and moments occurring at the crutch cuff, handle, and tip can now be measured with the use of advanced sensor technology.[19] To our knowledge, these new endeavors are the upmost accurate and reliable presentation of UE kinetic data of the shoulder, elbow and wrist joints in children with OI using Lofstrand crutches. Applications of this system may offer valuable insight for crutch prescription, gait pattern selection, and long-term usage effects.

METHODS

Kinematic Model

The UEs were modeled using seven rigid body segments (i.e., thorax, upper arms, forearms, and hands) and 28 retro-reflective markers placed on bony landmarks and Lofstrand crutches.[19] Vicon BodyBuilder software (Vicon, Oxford, England) was used for dynamic modeling.

Joint Centers

Joint centers were calculated using subject specific anthropometric data.[19,20] The thorax model was based on the results of work done by Nyugen et al., for analyzing thorax kinematics in children with myelomeningocele.[21] The markers located at the clavicles ($\overline{m}_{rclav}$ and $\overline{m}_{lclav}$), C7 spinous process ($\overline{m}_{spc7}$) and xiphoid process ($\overline{m}_{xi}$) were used to define the thorax movement. The thorax center ($\overline{t}_c$) was located halfway between the center of the clavicles and the C7 spinous process.

The upper arm was defined using markers placed on the acromion processes ($\overline{m}_{racr}$ and $\overline{m}_{lacr}$), and right and left medial ($\overline{m}_{rme}$ and $\overline{m}_{lme}$) and lateral elbow epicondyles ($\overline{m}_{rle}$ and $\overline{m}_{lle}$). The radius of the shoulder joint was estimated by measuring the circumference of the shoulder. The shoulder joint center ($\overline{s}_c$) was computed by subtracting the distance equal to the radius of the marker

(7 mm) summed with the radius of the shoulder (*r*) from the acromion process marker in the negative Y direction ($\overline{Y}$).

The forearm segment was defined by the right and left medial ($\overline{m}_{rme}$ and $\overline{m}_{lme}$) and lateral elbow epicondyles ($\overline{m}_{rle}$ and $\overline{m}_{lle}$), and the radial ($\overline{m}_{rrad}$ and $\overline{m}_{lrad}$) and ulnar styloids ($\overline{m}_{ru\ln}$ and $\overline{m}_{lu\ln}$). The midpoint of the medial and lateral epicondyles was defined as the elbow joint center ($\overline{e}_c$).

Similarly, the wrist segment was defined bilaterally by the radial ($\overline{m}_{rrad}$ and $\overline{m}_{lrad}$) and ulnar styloids ($\overline{m}_{ru\ln}$ and $\overline{m}_{lu\ln}$), 3rd metacarpal ($\overline{m}_{rm3}$ and $\overline{m}_{lm3}$), and 5th metacarpal ($\overline{m}_{rm5}$ and $\overline{m}_{lm5}$). The midpoint of the radial and ulnar styloids was defined as the wrist joint center ($\overline{w}_c$).

Segment Coordinate Systems

Segment coordinate systems were developed for each of the seven segments of the upper body and for each of the six segments of the crutches.[20] The relative motion between two adjacent segments was used to define the joint angles. ISB recommendations were implemented for developing the axes of the segment coordinate systems.[18] All coordinate axes followed the right hand rule, where the X-axis was directed anteriorly, the Y-axis was directed superiorly, and the Z-axis was directed laterally to the right. The vectors used to evaluate the axes of the segment coordinate systems are described below.

Thorax

The thorax coordinate system was designed using a temporary coordinate system and a virtual point.[21,22] The temporary coordinate system had its origin at the xiphoid process ($\overline{m}_{xiph}$). This temporary coordinate system was represented as

$$\overline{Y}_{temp} = \frac{\overline{m}_{spc7} - \overline{m}_{xiph}}{\left|\overline{m}_{spc7} - \overline{m}_{xiph}\right|} \quad (1)$$

$$\overline{X}_{temp} = \frac{\left(\overline{m}_{rclav} + \overline{m}_{lclav}\right)/2 - \overline{m}_{xiph}}{\left|\left(\overline{m}_{rclav} + \overline{m}_{lclav}\right)/2 - \overline{m}_{xiph}\right|} \times \overline{Y}_{temp} \quad (2)$$

$$\overline{Z}_{temp} = \overline{X}_{temp} \times \overline{Y}_{temp} \quad (3)$$

The virtual point ($\bar{t}_{virtualpoint}$) was then computed by translating the thorax center 10 mm in the direction of the temporary X-axis.

$$\bar{t}_{virtualpoint} = \overline{t}_c + 0.01 \times \overline{X}_{temp} \quad (4)$$

The thorax center ($\overline{t}_c$) was the origin for the thorax coordinate system.

$$\overline{X}_{Thorax} = \frac{\left(\overline{m}_{rclav} + \overline{m}_{lclav}\right)/2 - \overline{m}_{spc7}}{\left|\left(\overline{m}_{rclav} + \overline{m}_{lclav}\right)/2 - \overline{m}_{spc7}\right|} \quad (5)$$

$$\overline{Y}_{Thorax} = \frac{\bar{t}_{virtualpoint} - \bar{t}_c}{\left|\bar{t}_{virtualpoint} - \bar{t}_c\right|} \times \overline{X}_{Thorax} \quad (6)$$

$$\overline{Z}_{Thorax} = \overline{X}_{Thorax} \times \overline{Y}_{Thorax} \quad (7)$$

Upper Arm

The shoulder joint center ($\overline{s}_c$) was the origin for the upper arm segment coordinate system. The vectors defining this segment coordinate system were

$$\overline{Y}_{Upperarm} = \frac{\bar{s}_c - \bar{e}_c}{\left|\bar{s}_c - \bar{e}_c\right|} \quad (8)$$

$$\overline{Z}_{Upperarm} = \frac{\overline{m}_{uln} - \bar{e}_c}{\left|\overline{m}_{uln} - \bar{e}_c\right|} \times \overline{Y}_{Upperarm} \quad (9)$$

$$\overline{X}_{Upperarm} = \overline{Z}_{Upperarm} \times \overline{Y}_{Upperarm} \quad (10)$$

Forearm

The elbow joint center ($\overline{e_c}$) was the origin for the forearm segment coordinate system. Varus and valgus was constrained by methods similar to those reported by Hingtgen, et al., Rab et al., and Schmidt et al.[23-25] The equations defining the axes of this segment coordinate system were

$$\overline{Y}_{Forearm} = \frac{\overline{e}_c - \overline{m}_{u\ln}}{\left|\overline{e}_c - \overline{m}_{u\ln}\right|} \tag{11}$$

$$\overline{X}_{Forearm} = \frac{\overline{m}_{u\ln} - \overline{m}_{rad}}{\left|\overline{m}_{u\ln} - \overline{m}_{rad}\right|} \times \overline{Y}_{Forearm} \tag{12}$$

$$\overline{Z}_{Forearm} = \overline{X}_{Forearm} \times \overline{Y}_{Forearm} \tag{13}$$

Hand

The hand coordinate system was set up using a temporary coordinate system and a virtual point. The temporary coordinate system had its origin at the ulnar styloid ($\overline{m}_{u\ln}$). This temporary coordinate system was

$$\overline{Y}_{temp} = \frac{\overline{m}_{u\ln} - \overline{m}_{m5}}{\left|\overline{m}_{u\ln} - \overline{m}_{m5}\right|} \tag{14}$$

$$\overline{X}_{temp} = \frac{\overline{m}_{u\ln} - \overline{m}_{rad}}{\left|\overline{m}_{u\ln} - \overline{m}_{rad}\right|} \times \overline{Y}_{temp} \tag{15}$$

$$\overline{Z}_{temp} = \overline{X}_{temp} \times \overline{Y}_{temp} \tag{16}$$

The virtual point ($\overline{h}_{virtualpoint}$) was computed by translating the third metacarpal marker in the direction of the temporary X-axis by a distance equivalent to half of the subject specific width of the hand ($w/2$) and radius of the marker (7 mm).

$$\overline{h}_{virtualpoint} = \overline{m_{m3}} + \left(\frac{w}{2} + 0.007\right) \times \overline{X}_{temp} \tag{17}$$

The wrist center ($\overline{w_c}$) was the origin for the hand coordinate system.[18,26] The 3-D hand coordinate system was calculated as

$$\overline{Y}_{Hand} = \frac{\overline{w}_c - \overline{h}_{virtualpoint}}{\left|\overline{w}_c - \overline{h}_{virtualpoint}\right|} \tag{18}$$

$$\overline{X}_{Hand} = \frac{\overline{m}_{u\ln} - \overline{m}_{rad}}{\left|\overline{m}_{u\ln} - \overline{m}_{rad}\right|} \times \overline{Y}_{Hand} \tag{19}$$

$$\overline{Z}_{Hand} = \overline{X}_{Hand} \times \overline{Y}_{Hand} \tag{20}$$

Crutch

Each Lofstrand crutch was divided into three segments: lower crutch, crutch handle, and crutch cuff (Figure 2).[19,20] The crutch was modeled as a rigid body segment. Thus, one main crutch segment was defined, which was then appropriately modified using spatial coordinate transformation for the computation of segmental kinematics.

Handle

The crutch handle segment consisted of the crutch handle, the upper load cell and the lower load cell. The crutch maker setup is shown in Figure 2. The origin of the handle segment ($\overline{lc}_c$) was defined as the midpoint of the lower load cell. The midpoint of the crutch tip was computed as a virtual point ($\overline{c}_{\text{virtualpoint}}$), which was then used for defining the segment coordinate system.[19]

$$\overline{lc}_c = \frac{(\overline{m}_{lateral} + \overline{m}_{medial})}{2} \tag{21}$$

$$\overline{c}_{virtualpo\,\text{int}} = \frac{(\overline{m}_{anterior} + \overline{m}_{posterior})}{2} \tag{22}$$

$$\overline{Y}_{Handle} = \frac{\overline{lc}_c - \overline{c}_{virtualpoint}}{\left|\overline{lc}_c - \overline{c}_{virtualpoint}\right|} \tag{23}$$

$$\overline{X}_{Handle} = \frac{\overline{m}_{medial} - \overline{m}_{lateral}}{\left|\overline{m}_{medial} - \overline{m}_{lateral}\right|} \times \overline{Y}_{Handle} \quad (24)$$

$$\overline{Z}_{Handle} = \overline{X}_{Handle} \times \overline{Y}_{Handle} \quad (25)$$

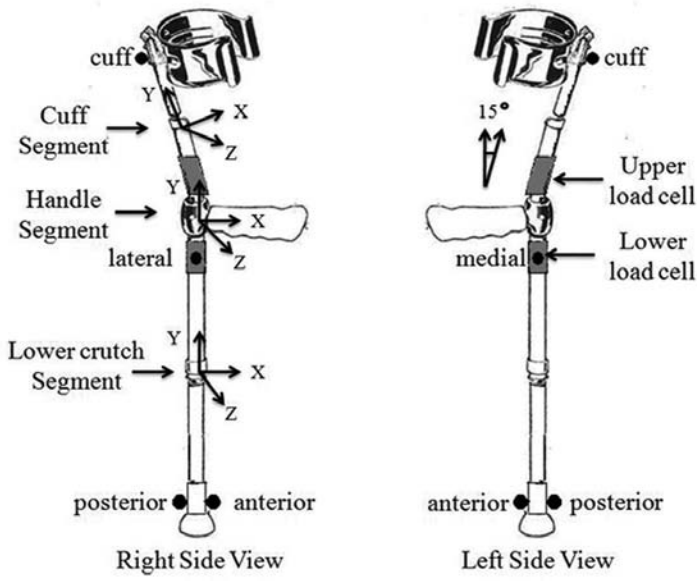

Figure 2. Crutch segment definitions and axes orientation. Each crutch segment consists of the handle, the lower crutch, and cuff segments. The coordinate systems of the segments follow x-axis: anterior, y-axis: superior, and z-axis: lateral. The cuff is offset from the lower crutch by a 15-degree angle. Markers were placed on the cuff segment, right and left sides of the lower load cell, and on the anterior and posterior crutch tip. (Reprinted from Journal of Biomechanics, 44 (11), Brooke A. Slavens, Neha Bhagchandani, Mei Wang, Peter A. Smith, and Gerald F. Harris, An upper extremity inverse dynamics model for pediatric Lofstrand crutch-assisted gait, Copyright 2011, with permission from Elsevier.[19])

Lower crutch

The midpoint of the lower load cell ($\overline{lc}_c$) and the virtual point ($\overline{c}_{\text{virtualpoint}}$) was used to compute the origin for the crutch tip segment ($\overline{Ctip}_c$).[19]

$$\overline{Ctip}_c = \frac{(\overline{lc}_c + \overline{c}_{virtualpoint})}{2} \quad (26)$$

$$\overline{Y}_{LowerCrutch} = \frac{\overline{lc}_c - \overline{Ctip}_c}{\left|\overline{lc}_c - \overline{Ctip}_c\right|} \quad (27)$$

$$\overline{X}_{LowerCrutch} = \frac{\overline{m}_{medial} - \overline{m}_{lateral}}{\left|\overline{m}_{medial} - \overline{m}_{lateral}\right|} \times \overline{Y}_{LowerCrutch} \quad (28)$$

$$\overline{Z}_{LowerCrutch} = \overline{X}_{LowerCrutch} \times \overline{Y}_{LowerCrutch} \quad (29)$$

Cuff

To define the cuff coordinate system, a temporary segment was first designed, which was positively rotated along the Z-axis by an angle of 15 degrees. The 15-degree angle is attributed to the cuff being rotated 15 degrees with reference to the vertical shaft (Figure 2). To obtain the origin of the cuff segment, the midpoint of the upper load cell was estimated by translating the lower load cell midpoint by 9 cm in the Y direction of the temporary axis. The cuff segment had the same orientation as the temporary axis while the origin of this coordinate system was located at the midpoint of the upper load cell. The temporary axis definitions, origin of the cuff segment, and the axes of the coordinate system of the cuff segment are given below.[19]

$$\overline{Z}_{temp} = \overline{Z}_{Handle} \quad (30)$$

$$\overline{X}_{temp} = \overline{X}_{Handle} * \cos(15^o) - \overline{Y}_{Handle} * \sin(15^o) \quad (31)$$

$$\overline{Y}_{temp} = \overline{X}_{Handle} * \sin(15^o) + \overline{Y}_{Handle} * \cos(15^o) \quad (32)$$

$$\overline{cuff}_c = \left(\overline{lc}_c + 0.09\right) \times \overline{Y}_{temp} \quad (33)$$

$$\overline{Z}_{cuff} = \overline{Z}_{temp} \quad (34)$$

$$\overline{X}_{cuff} = \overline{X}_{temp} \quad (35)$$

$$\overline{Y}_{cuff} = \overline{Y}_{temp} \quad (36)$$

Euler Angle Sequence

The Z-X-Y Euler rotation sequence was used to evaluate the UE joint kinematics.[27]

$$R = \begin{bmatrix} -\sin(\theta_1)\sin(\theta_2)\sin(\theta_3)+\cos(\theta_1)\cos(\theta_3) & -\sin(\theta_1)\cos(\theta_2) & \sin(\theta_1)\sin(\theta_2)\cos(\theta_3)+\cos(\theta_1)\sin(\theta_3) \\ \cos(\theta_1)\sin(\theta_2)\sin(\theta_3)+\sin(\theta_1)\cos(\theta_3) & \cos(\theta_1)\cos(\theta_2) & -\cos(\theta_1)\sin(\theta_2)\cos(\theta_3)+\sin(\theta_1)\sin(\theta_3) \\ -\cos(\theta_2)\sin(\theta_3) & \sin(\theta_2) & \cos(\theta_2)\cos(\theta_3) \end{bmatrix} \quad (37)$$

Kinetic Model

Lofstrand crutches (Walk Easy, Inc., Delray Beach, FL) were instrumented with four six-degree-of-freedom, custom designed load cells (2 per crutch; AMTI, Watertown, MA). One transducer each was placed above and below the crutch handle to directly measure triaxial forces and moments. The analog data from the load cells were amplified using AMTI MSA-6 high gain amplifiers. The weight of each load cell and crutch was 0.10 kg and 0.43 kg, respectively.

Kinetic Equations

The kinetic equations were computed using the inverse dynamics Newton-Euler approach.[27] Reaction forces and moments from the two load cells in each crutch were used recursively to solve the kinetic equations one after the other, starting from the most distal segment. The proximal forces were computed from the known distal forces, mass, and acceleration of a segment. The proximal moments were computed from the known distal moments, rate of change of angular momentum of the segment, moment arms, and moment contribution of the distal and proximal forces. The free body diagrams for each segment are displayed (Figures 3-5). The kinetic equations for each segment were applied separately in the x, y and z directions.

Lower Crutch Segment

The lower crutch segment consisted of the lower load cell and the lower shaft of the crutch. The force and moment from the lower load cell were used to evaluate the force and moment contribution at the crutch tip (Figure 3) as

$$\overline{F}_{ctip} = -m_{ctip}(\overline{a}_{ctip} + \overline{g}) - \overline{F}_{lowerLC} \quad (38)$$

$$\overline{M}_{ctip} = \dot{H}_{ctip} - \overline{M}_{lowerLC} - \overline{r}_{dist} \times \overline{F}_{ctip} - \overline{r}_{prox} \times \overline{F}_{lowerLC} \quad (39)$$

where $\overline{F}_{ctip}$ and $\overline{M}_{ctip}$ are the unknown force and moment occurring at the crutch tip. m_{ctip} and $\bar{a}_{ctip}$ are the mass and the linear acceleration of the lower crutch segment. $\bar{g}$ is the acceleration due to gravity. $\overline{F}_{lowerLC}$ and $\overline{M}_{lowerLC}$ are the known force and moment at the lower load cell. $\dot{H}_{ctip}$ is zero since the angular velocities and accelerations are zero for a rigid body. $\bar{r}_{dist}$ is the distance from the crutch tip and $\bar{r}_{prox}$ is the distance from the center of the lower load cell to the center of mass (CoM) of the lower segment.[19]

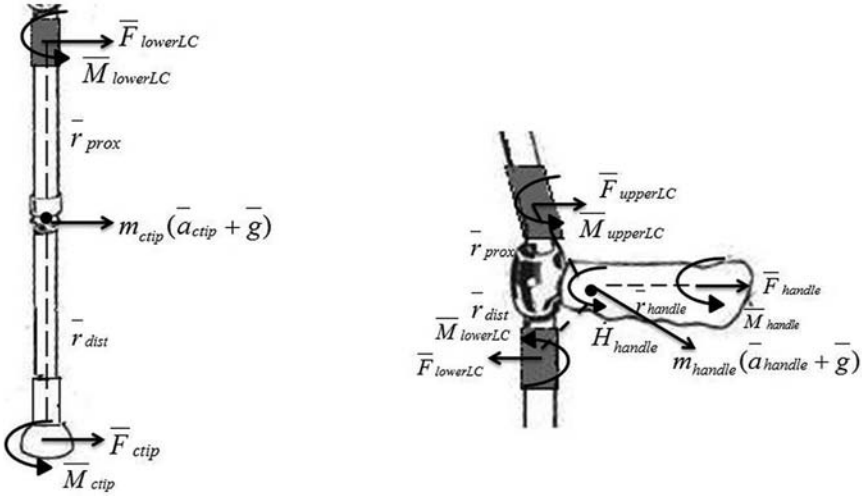

Figure 3. Kinetic model of the lower crutch and crutch handle segments. (Reprinted from Journal of Biomechanics, 44 (11), Brooke A. Slavens, Neha Bhagchandani, Mei Wang, Peter A. Smith, and Gerald F. Harris, An upper extremity inverse dynamics model for pediatric Lofstrand crutch-assisted gait, Copyright 2011, with permission from Elsevier.[19])

Handle Segment

The handle segment consists of the crutch handle, and the lower and upper load cells. The force and moment from the lower and upper load cells were used to determine the force and moment contribution at the handle (Figure 3). These terms are

$$\overline{F}_{handle} = -m_{handle}(\bar{a}_{handle} + \bar{g}) + \overline{F}_{lowerLC} - \overline{F}_{upperLC} \tag{40}$$

$$\overline{M}_{handle} = \dot{H}_{handle} + \overline{M}_{lowerLC} - \overline{M}_{upperLC} + \bar{r}_{dist} \times \overline{F}_{lowerLC} - \bar{r}_{prox} \times \overline{F}_{upperLC} - \bar{r}_{handle} \times \overline{F}_{handle} \tag{41}$$

where $\overline{F}_{handle}$ and $\overline{M}_{handle}$ are the unknown force and moment occurring at the point of contact between the hand the crutch handle. m_{handle} and $\bar{a}_{handle}$ are the mass and the linear acceleration of the handle segment. $\overline{F}_{lowerLC}$ and $\overline{M}_{lowerLC}$ are the known force and moment at the lower load cell. $\overline{F}_{upperLC}$ and $\overline{M}_{upperLC}$ are the known force and moment at the upper load cell. $\dot{H}_{handle}$ is the rate of change of angular momentum of the handle segment. $\bar{r}_{dist}$ is the distance from the CoM of the lower load cell, $\bar{r}_{prox}$ is the distance from the CoM of the upper load cell and $\bar{r}_{handle}$ is the distance from the point of contact of the hand on the crutch handle to the CoM of the handle segment.[19]

Cuff Segment

The cuff segment consisted of the upper load cell and the cuff. The force and moment from the upper load cell were used to calculate the force and moment contribution at the cuff (Figure 4) as

$$\overline{F}_{cuff} = -m_{cuff}(\bar{a}_{cuff} + \bar{g}) + \overline{F}_{upperLC} \tag{42}$$

$$\overline{M}_{cuff} = \dot{H}_{cuff} - \overline{M}_{upperLC} + \bar{r}_{dist} \times \overline{F}_{upperLC} - \bar{r}_{prox} \times \overline{F}_{cuff} \tag{43}$$

where $\overline{F}_{cuff}$ and $\overline{M}_{cuff}$ are the unknown force and moment occurring at the point of contact of the cuff. m_{cuff} and $\bar{a}_{cuff}$ are the mass and the linear acceleration of the cuff segment. $\overline{F}_{upperLC}$ and $\overline{M}_{upperLC}$ are the known force and moment at the upper load cell. $\dot{H}_{cuff}$ is zero since the angular velocities and accelerations are zero for a rigid body. $\bar{r}_{dist}$ is the distance from the CoM of the upper load cell and $\bar{r}_{prox}$ is the distance from the point of contact at the cuff to the CoM of the cuff segment.[19]

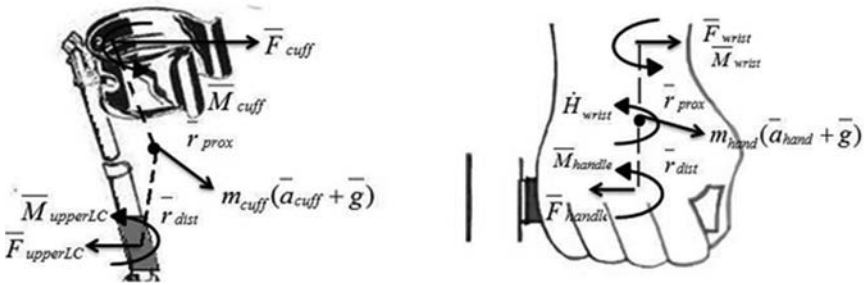

Figure 4. Kinetic model of the crutch cuff and hand segments. (Reprinted from Journal of Biomechanics, 44 (11), Brooke A. Slavens, Neha Bhagchandani, Mei Wang, Peter A. Smith, and Gerald F. Harris, An upper extremity inverse dynamics model for pediatric Lofstrand crutch-assisted gait, Copyright 2011, with permission from Elsevier.[19])

Hand Segment

The force and moment from the lower load cell were used to evaluate the force and moment contribution at the wrist (Figure 4). These terms are

$$\overline{F}_{wrist} = -m_{hand}(\bar{a}_{hand} + \bar{g}) + \overline{F}_{handle} \tag{44}$$

$$\overline{M}_{wrist} = \dot{H}_{wrist} + \overline{M}_{handle} + \bar{r}_{dist} \times \overline{F}_{handle} - \bar{r}_{prox} \times \overline{F}_{wrist} \tag{45}$$

where $\overline{F}_{wrist}$ and $\overline{M}_{wrist}$ are the unknown force and moment occurring at the wrist joint. m_{wrist} and $\bar{a}_{wrist}$ are the mass and the linear acceleration of the wrist segment. $\overline{F}_{handle}$ and $\overline{M}_{handle}$ are the known force and moment at the point of contact between the hand and crutch handle. $\dot{H}_{wrist}$ is the rate of change of angular momentum of the wrist segment. $\bar{r}_{dist}$ is the distance from the point of contact between the hand and crutch handle and $\bar{r}_{prox}$ is the distance from the wrist joint center to the CoM of the wrist segment.[19]

Forearm Segment

The force and moment from the wrist joint and the point of contact at the cuff were used to compute the force and moment at the elbow (Figure 5) as

$$\overline{F}_{elbow} = -m_{forearm}(\bar{a}_{forearm} + \bar{g}) + \overline{F}_{wrist} + \overline{F}_{cuff} \tag{46}$$

$$\overline{M}_{elbow} = \dot{H}_{elbow} + \overline{M}_{wrist} + \overline{M}_{cuff} + r_{dist} \times \overline{F}_{wrist} + r_{cuff} \times \overline{F}_{cuff} - r_{prox} \times \overline{F}_{wrist} \tag{47}$$

where $\overline{F}_{elbow}$ and $\overline{M}_{elbow}$ are the unknown force and moment occurring at the elbow joint. m_{elbow} and $\bar{a}_{elbow}$ are the mass and the linear acceleration of the forearm segment. $\overline{F}_{wrist}$ and $\overline{M}_{wrist}$ are the known force and moment at the wrist joint. $\overline{F}_{cuff}$ and $\overline{M}_{cuff}$ are the known force and moment at the point of contact of the cuff. $\dot{H}_{elbow}$ is the rate of change of angular momentum of the elbow joint. $\bar{r}_{dist}$ is the distance from the wrist joint center, $\bar{r}_{prox}$ is the distance from the elbow joint center and $\bar{r}_{cuff}$ is the distance from the point of contact at the cuff to the CoM of the elbow segment.[19]

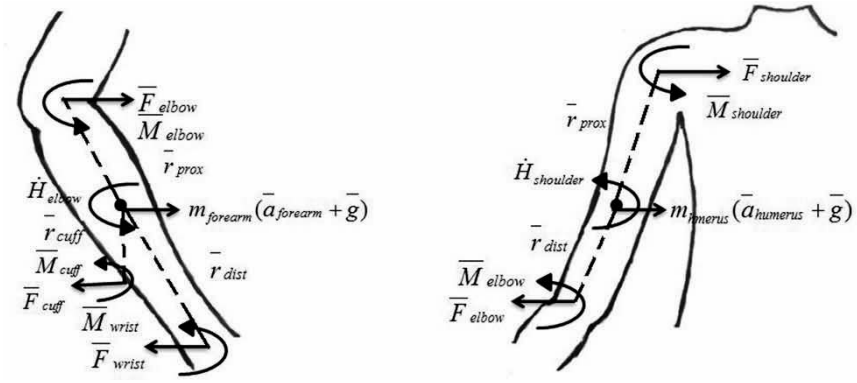

Figure 5. Kinetic model of the forearm and upper arm segments. (Reprinted from Journal of Biomechanics, 44 (11), Brooke A. Slavens, Neha Bhagchandani, Mei Wang, Peter A. Smith, and Gerald F. Harris, An upper extremity inverse dynamics model for pediatric Lofstrand crutch-assisted gait, Copyright 2011, with permission from Elsevier.[19])

Upper Arm Segment

The upper arm segment consisted of the humerus. The force and moment from the elbow joint were used to calculate the force and moment contribution at the shoulder (Figure 5), which are

$$\overline{F}_{shoulder} = -m_{humerus}\left(\bar{a}_{humerus} + \bar{g}\right) + \overline{F}_{elbow} \tag{48}$$

$$\overline{M}_{shoulder} = \dot{H}_{shoulder} + \overline{M}_{elbow} + \bar{r}_{dist} \times \overline{F}_{elbow} - \bar{r}_{prox} \times \overline{F}_{shoulder} \tag{49}$$

where $\overline{F}_{shoulder}$ and $\overline{M}_{shoulder}$ are the unknown force and moment occurring at the shoulder joint. $m_{humerus}$ and $\bar{a}_{humerus}$ are the mass and the linear

acceleration of the upper arm segment. $\overline{F}_{elbow}$ and $\overline{M}_{elbow}$ are the known force and moment at the elbow joint. $\dot{H}_{shoulder}$ is the rate of change of angular momentum of the shoulder joint. $\bar{r}_{dist}$ is the distance from the elbow joint center and $\bar{r}_{prox}$ is the distance from the shoulder joint center to the CoM of the upper arm segment.[19]

System Evaluation

Static evaluation was conducted by applying two pound loads along the three primary axes of the instrumented crutches at the shaft and the forearm cuff while the crutch was supported by an alignment device to independently evaluate each 6-axis load cell. Dynamic evaluation of the system was then performed by having a normal subject walk with the instrumented crutches over a calibrated force plate, which was similar to previous validation methods.[19,26,28] The resultant forces measured by both systems were calculated. Percentage root mean square (RMS) error and standard deviation (SD) from five trials was computed for static and dynamic evaluations to determine system accuracy and precision.[19]

Subject Demonstration

A female subject with type I OI (age: 16 yrs, height: 1.4 m, weight: 44 kg) participated in the study after acquiring written parental consent and subject assent in compliance with Shriners Hospitals for Children-Chicago's Institutional Review Board (IRB) requirements. Exclusion criteria included orthopaedic surgery in the last one-year or a fracture in the last six months. The instrumented Lofstrand crutches were adjusted to match the height and cuff size of the subject's current crutches. A 14-camera Vicon motion analysis system (Vicon, Oxford, England) recorded the subject ambulating with the kinetic Lofstrand crutches and the marker system on a six-meter walkway at a self-selected pace and gait pattern (two-point reciprocal gait pattern). The kinematic data were sampled at 120 Hz and filtered with a Woltring filter. The gait cycle was normalized from heel strike to heel strike and averaged over six trials. Matlab (MathWorks Inc., Natick, MA) was used for post-processing. Joint reaction forces and moments were computed and normalized to % body weight (% BW) and % body weight multiplied by height (% BW*H), respectively.

Data Collection and Analysis

Mean cadence, walking speed, stride length, and stance duration were determined from the lower extremity kinematics data. Motions of the crutch, thorax, shoulder, elbow, and wrist were evaluated three-dimensionally. The range of motion (ROM) was computed as the difference of the maximum and minimum motions. Mean external forces and moments at the crutch tip, handle, and cuff were computed. Mean joint reaction forces and joint reaction moments were calculated bilaterally for the wrist, elbow, and shoulder. Forces were normalized to percent body weight (% BW) and moments were normalized to percent body weight times height (% BW*H). Peak forces and moments were defined as the absolute maximum forces and moments during the gait cycle, respectively.

RESULTS

System Evaluation

The % RMS error and standard deviation (SD) in the sagittal plane during static validation were most notable (Table 1). The smallest error of 0.84% RMS was documented in the inferior force of the lower right load cell. The smallest SD of 0.001 N was documented in the fore tilt moment of the lower left load cell. The left crutch presented a smaller error and SD than the right crutch during dynamic validation against the force plate (Table 2).

Table 1. Static evaluation of the crutch sensor system measured by root mean square (RMS) error and standard deviation (SD).[19]

Forces and moments	Root mean square error (%)		Standard deviation (N)	
	Right	Left	Right	Left
Upper load cell: inferior force	4.06	1.11	0.11	0.04
Upper load cell: fore tilt moment	4.09	4.76	0.001	0.05
Lower load cell: inferior force	0.84	0.90	0.05	0.05
Lower load cell: fore tilt moment	3.74	5.20	0.03	0.001

Table 2. Dynamic evaluation of the right and left crutch load cells resultant force measured by root mean square (RMS) error and standard deviation (SD).[19]

Resultant force	Root mean square error (%)		Standard deviation (N)	
	Right	Left	Right	Left
	2.81	1.43	0.55	0.29

Kinematics

The subject presented with 103 steps/min cadence, 0.78 m/s walking speed, 0.91 m stride length, and a stance duration of 65%. Cadence, walking speed, and stride length were relatively high as compared with other crutch-user pathologies.[19] Kinematic curves are presented for the crutches and UEs for the primary weight bearing extremity (Figure 6).

Crutches

The subject demonstrated crutch fore tilt for 0-30% of the gait cycle, followed by aft tilt for the rest of the gait cycle (Figure 6). Throughout the gait cycle, the crutches were titled laterally and internally rotated. Crutch ROM in the sagittal plane was 31 degrees.

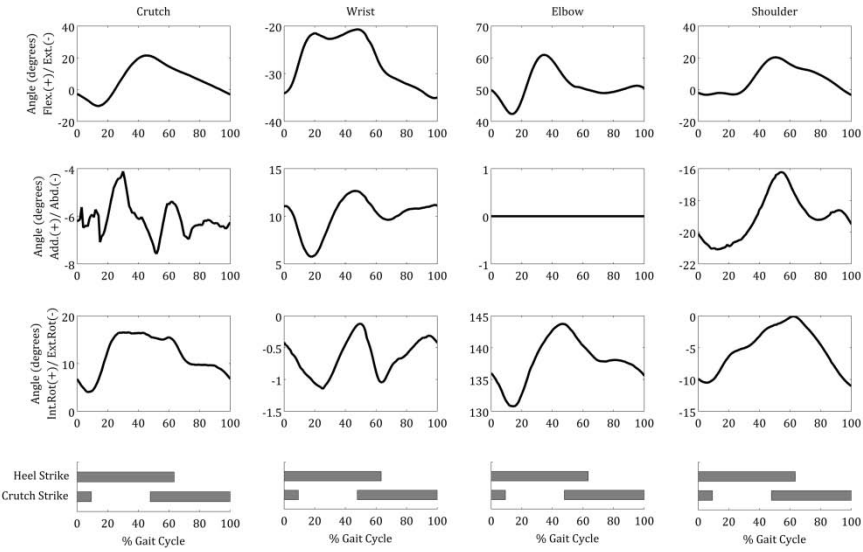

Figure 6. Crutch, wrist, elbow, and shoulder joint motions for the primary weight bearing extremity (right side) from 0-100% of the gait cycle .

Wrist

The wrist demonstrated the smallest ROM of the UE joints (Figure 6). Wrist kinematics displayed extension, adduction and external rotation for the entire gait cycle. Wrist ROM in the sagittal plane was 14 degrees.

Elbow

The elbow moved in flexion and internal rotation throughout the gait cycle (Figure 6). The elbow was constrained in the coronal plane. Elbow ROM in the sagittal plane was 18 degrees.

Shoulder

The shoulder demonstrated the largest ROM of the UE joints (Figure 6). Shoulder ROM in the sagittal plane was 24 degrees. Sagittal plane shoulder motion displayed extension from 0-30% of gait cycle, which was followed by flexion until the end of the gait cycle. Shoulder motion remained abducted and externally rotated during the gait cycle.

Thorax

The frontal plane showed the greatest ROM for the thorax in lateral bending (Figure 6). Sagittal plane motion presented as flexion throughout the gait cycle. The subject demonstrated clockwise rotation for 0-40% of the gait cycle, followed by counterclockwise rotation for rest of the gait cycle.

Kinetics

The subject presented a primary weight bearing extremity (right leg), which showed more significant, higher joint reaction forces and moments than the contralateral extremity. Kinetic forces and moments of the crutches, shoulder, elbow and wrist for the right side are depicted (Figures 7-10).

Crutch

Forces and moments were measured at the crutch tip, handle, and cuff for improved accuracy from previous models. Due to the calibration procedure, all forces were zero when the crutch was off the ground.

Crutch tip

Crutch tip forces were minimal in the anterior/posterior and medial/lateral directions (Figure 7). The largest crutch tip forces occurred in the inferior direction, with a peak of 21% BW. Crutch tip abduction moments were largest followed by extension moments (Figure 8). Internal and external rotation moments were minimal.

Crutch handle

The largest forces at the crutch handle were directed superiorly (Figure 7). Peak superior force was 16% BW. Lateral and posterior forces were also present. Cuff moments presented relatively similar magnitudes for extension, adduction, and internal rotation (Figure 8).

Crutch cuff

Anteriorly directed forces were the largest forces at the cuff (Figure 7). The peak anterior force was 4.3% BW. The cuff forces were also directed laterally, superiorly, and inferiorly. Cuff moments were minimal in all planes, showing extension, adduction, and external rotation (Figure 8).

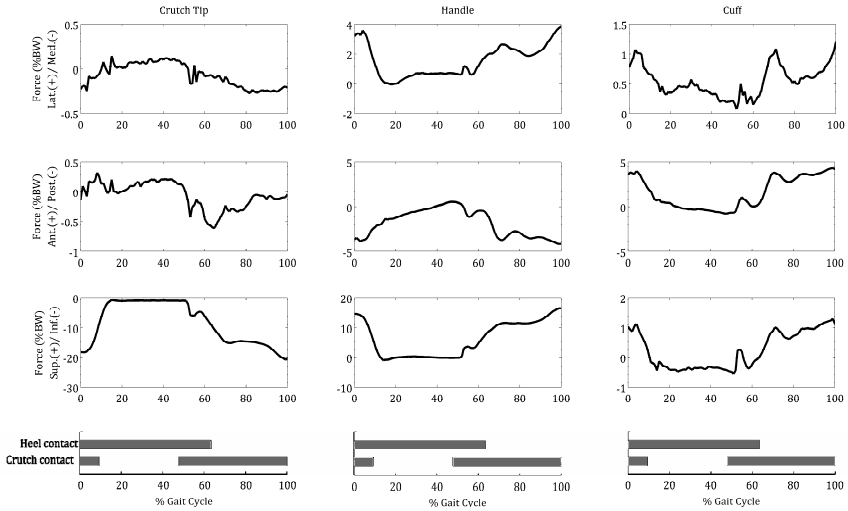

Figure 7. Crutch tip, handle, and cuff reaction forces for the primary weight bearing extremity (right side) from 0-100% of the gait cycle. Forces are normalized to percent body weight (% BW).

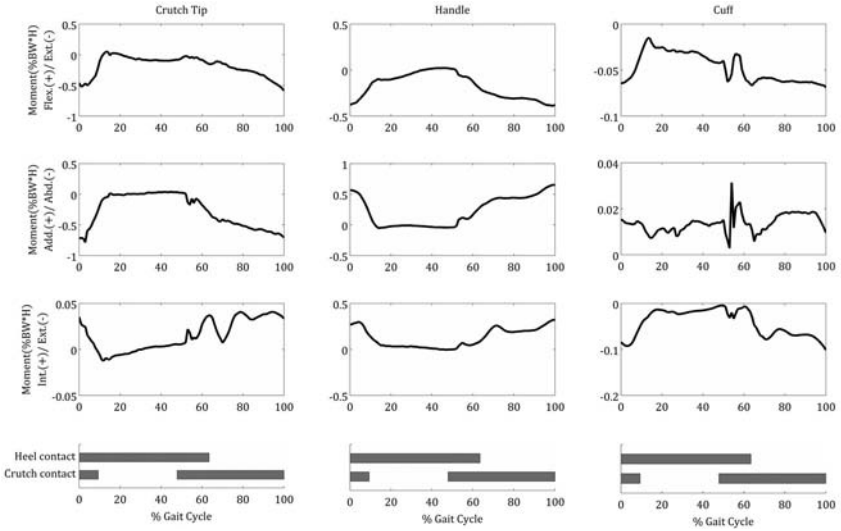

Figure 8. Crutch tip, handle, and cuff reaction moments for the primary weight bearing extremity (right side) from 0-100% of the gait cycle. Moments are normalized to percent body weight multiplied by height (% BW*H).

Wrist

Wrist joint reaction forces presented medially, posteriorly, and superiorly during the gait cycle (Figure 9). The largest peak forces were 15% BW and were directed posteriorly. The wrist joint reaction moments presented in the directions of flexion, adduction, and internal rotation (Figure 10). The peak wrist moment was 0.7 % BW*H.

Elbow

The elbow displayed the largest joint reaction forces of all UE joints (Figure 9). The elbow joint reaction forces were largest in the superior direction with a peak of 15% BW. Forces were also directed posteriorly during crutch contact, anteriorly during heel contact, and medially throughout the gait cycle. The largest moment at the elbow was the adduction moment (1.1% BW*H), followed by the extension moment, and then the internal rotation moment (Figure 10).

Shoulder

The shoulder joint showed forces in all directions (Figure 9). The largest shoulder joint forces were in the superior direction, with a peak of 9% BW.

The flexion moment was the largest shoulder joint reaction moment, followed by the abduction moment, and external rotation moment (Figure 10). The peak flexion shoulder moment was 1.9 % BW*H. The shoulder had the largest moments of all UE joints.

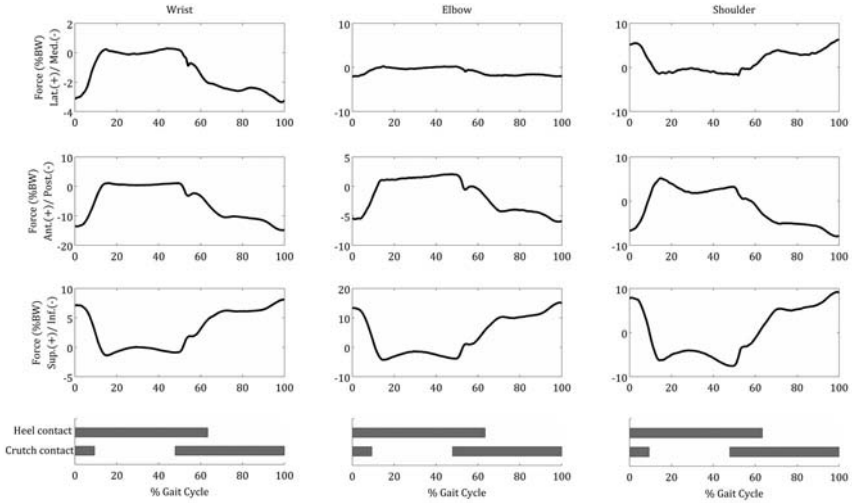

Figure 9. Wrist, elbow, and shoulder joint reaction forces for the primary weight bearing extremity (right side) from 0-100% of the gait cycle. Forces are normalized to percent body weight (% BW).

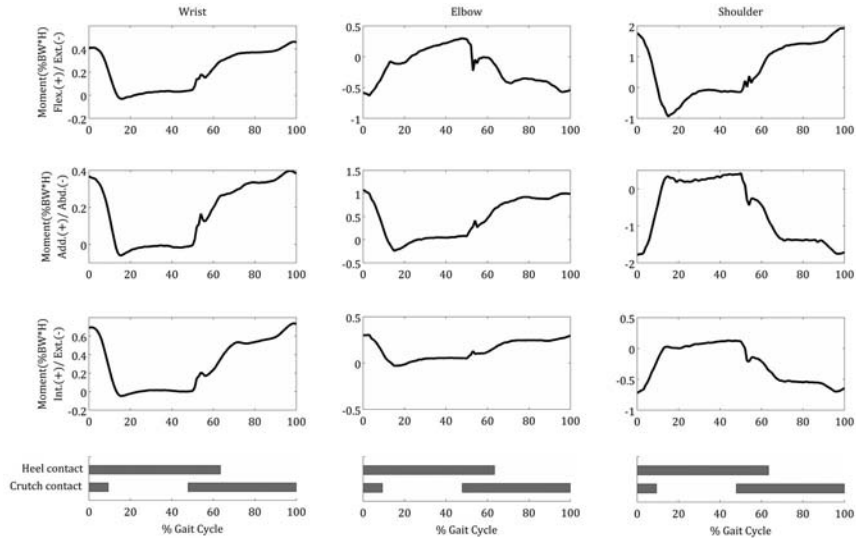

Figure 10. Wrist, elbow, and shoulder joint reaction moments for the primary weight bearing extremity (right side) from 0-100% of the gait cycle. Moments are normalized to percent body weight multiplied by height (% BW*H).

DISCUSSION

Upper extremity movement assessment in children with OI has been limited. Nonetheless, UE model development and application to assisted gait has been of great interest to our group. Slavens et al. designed the first generation Lofstrand crutch model for evaluation of UE dynamics in children with myelomeningocele.[22,28] This ISB compliant model used 26 markers and a kinetic Lofstrand crutch system to acquire 3-D shoulder, elbow, and wrist joint forces and moments. Hardware limitations only allowed single force transducers to be placed at the distal end of the Lofstrand crutches to capture 3-D reaction forces and moments. This model was applied to nine subjects with myelomeningocele for comparison of common Lofstrand crutch assisted gait patterns, including reciprocal gait and swing-through gait. Findings showed that swing-through gait placed the greatest forces on the shoulder and elbow joints, which were approximately 50% BW. Accurate quantitative assessment was shown to be essential for preventing injury in long-term crutch users. Results of this study led to a new Lofstrand crutch hardware design for further investigation of joint load demands on the UEs during assisted gait. New advances in hardware technology led us to our current research, incorporating dual sensors per crutch, for improved accuracy of joint kinetics. This system enabled the crutch cuff kinetics to be resolved. In addition, the newest design is lighter weight and has a reduced moment of inertia due to the location of the hardware components. The kinetic Lofstrand crutch system has been applied to children with orthopaedic disabilities for quantification of UE joint load demands.[19] Specifically, the application of this system to children with OI will help determine their risk for fracture, and may provide insight for ways to decrease joint loads during assisted gait.

This work supports the use of a technically validated inverse dynamics model to evaluate UE ambulation patterns of children with OI during Lofstrand crutch-assisted gait. The crutch system was utilized for characterizing 3-D joint kinematics and kinetics of the shoulder, elbow, and wrist. The superior joint forces at the shoulder and elbow, and the posterior wrist forces demonstrate the most significant findings concerning joint loading demands for this subject with OI. The flexion moment at the shoulder was the largest joint moment of the UEs. These joint forces and moments are of concern with long-term crutch usage in the OI population, since it has been shown that UE pain and pathology may develop.[10,13,15]

We hope to clinically utilize the UE dynamics results to identify potential kinetic risk factors for the OI population. Our goal is to minimize skeletal loads in an effort to reduce fracture risk in children with OI. Through the use of advanced inverse dynamics models, along with computational modeling such as finite element and musculoskeletal modeling, new prediction tools may be developed to predict or prevent bone fractures. Advanced modeling techniques may also lead to innovative assistive device design and development. Improved crutch designs may allow one to be alerted when reaching concerning load levels. Alternative crutch cuff and handle designs may also be implemented to further reduce loading on the UE joints.

CONCLUSION

We conclude that the 3-D kinetic Lofstrand crutch system is useful for quantifying UE joint motions, forces, and moments during assisted gait. Risk factors for UE joint pathology may be identified using this kinetic system. The inverse dynamics model may be used to better understand joint load optimization through activity modification, gait training, and crutch re-design. This research may ultimately improve crutch prescription, therapeutic gait planning, and offer insight to longer-term joint loading effects in children with OI.

ACKNOWLEDGEMENTS

We would like to thank Adam Graf, Joe Krzak, and Kathy Reiners for their help with this work. The contents of this chapter were developed under a grant from the Department of Education, NIDRR grant number H133E100007. However, those contents do not necessarily represent the policy of the Department of Education, and one should not assume endorsement by the Federal Government.

REFERENCES

1. Kaye HS, Kang T, LaPlante MP. Mobility device use in the United States. *Disability Statistics Report (14)*. Washington, D.C.: U.S. Department of Education, National Institute on Disability and Rehabilitation Research; 2000.
2. Slavens BA, Frantz J, Sturm PF, Harris GF. Upper extremity dynamics during Lofstrand crutch-assisted gait in children with myelomeningocele. *Journal of Spinal Cord Medicine* 2007; 30: 77-83.
3. Slavens BA, Harris GF. The biomechanics of upper extremity kinematic and kinetic modeling: Applications to rehabilitation engineering. *Critical Reviews in Biomedical Engineering* 2008; 36(2-3): 93-125.

4. Slavens BA, Bhagchandani N, Wang M, Smith PA, Harris GF. Motion analysis of the upper extremities during lofstrand crutch-assisted gait in children with orthopaedic disabilities. *Journal of Experimental & Clinical Medicine* 2011; 3(5): 218-227.
5. Harris GF, Smith PA. *Human motion analysis*. New York: IEEE Press; 1996.
6. Slavens BA, Harris GF. Biomechanics. In: Abu-Faraj ZO, ed. *Handbook of research on biomedical engineering education and advanced bioengineering learning: Interdisciplinary concepts*. Hershey, PA: IGI Global; 2012.
7. Gajko-Galicka A. Mutations in type I collagen genes resulting in osteogenesis imperfecta in humans. *Acta Biochimica Polonica* 2002; 49(2): 433-441.
8. Osteogenesis Imperfecta Foundation. Facts about osteogenesis imperfecta. 2007; http://www.oif.org/site/PageServer?pagename=AOI_Facts.
9. Byers PH, Steiner RD. Osteogenesis imperfecta. *Annual Review of Medicine* 1992; 43: 269-282.
10. Klimaitis A, Carroll G, Owen E. Rapidly progressive destructive arthropathy of the shoulder--a viewpoint on pathogenesis. *Journal of Rheumatology* 1988; *15(12):1859-62*.
11. Newsam CJ, Lee AD, Mulroy SJ, Perry J, Newsam CJ, Lee AD, et al. Shoulder emg during depression raise in men with spinal cord injury: The influence of lesion level. *Journal of Spinal Cord Medicine* 2003; 26(1): 59-64.
12. Sharkey NA, Marder RA. The rotator cuff opposes superior translation of the humeral head. *American Journal of Sports Medicine* 1995; 23(3): 270-275.
13. Lal S. Premature degenerative shoulder changes in spinal cord injury patients. *Spinal Cord* 1998; 36(3): 186-189.
14. Opila KA, Nicol AC, Paul JP. Upper limb loadings of gait with crutches. *Journal of Biomechanical Engineering* 1987; 109(4): 285-290.
15. Kellner WS, Felsenthal G, Anderson JM, Hilton EB, Mondell DL. Carpal tunnel syndrome in the nonparetic hands of hemiplegics. Stress-induced by ambulatory assistive devices. *Orthopaedic Review* 1986; 15(9): 608-611.
16. Sala DA, Leva LM, Kummer FJ, Grant AD. Crutch handle design: Effect on palmar loads during ambulation. *Archives of Physical Medicine and Rehabilitation* 1998; 79(11): 1473-1476.
17. Waring WP, Werner RA. Clinical management of carpal tunnel syndrome in patients with long-term sequelae of poliomyelitis. *Journal of Hand Surgery* 1989; 14(5): 865-869.
18. Wu G, van der Helm FC, Veeger HE, Makhsous M, Van Roy P, Anglin C, et al. ISB recommendation on definitions of joint coordinate systems of various joints for the reporting of human joint motion--part ii: Shoulder, elbow, wrist and hand. *Journal of Biomechanics* 2005; 38(5): 981-992.
19. Slavens BA, Bhagchandani N, Wang M, Smith PA, Harris GF. An upper extremity inverse dynamics model for pediatric lofstrand crutch-assisted gait. *Journal of Biomechanics* 2011; 44(11): 2162-2167.
20. Bhagchandani N. *Upper extremity kinetics during lofstrand crutch-assisted gait in children*. Milwaukee, WI: Biomedical Engineering, Marquette University; 2010.
21. Nguyen TC, Baker R. Two methods of calculating thorax kinematics in children with myelomeningocele. *Clinical Biomechanics* 2004; 19(10): 1060-1065.
22. Slavens BA, Sturm PF, Bajorunaite R, Harris GF. Upper extremity dynamics during Lofstrand crutch-assisted gait in children with myelomeningocele. *Gait & Posture* 2009; 30: 511-517.
23. Rab G, Petuskey K, Bagley A. A method for determination of upper extremity kinematics. *Gait & Posture* 2002; 15(2): 113-119.

24. Schmidt R, Disselhorst-Klug C, Silny J, Rau G. A marker-based measurement procedure for unconstrained wrist and elbow motions. *Journal of Biomechanics* 1999; 32(6): 615-621.
25. Hingtgen BA, McGuire JR, Wang M, Harris GF. An upper extremity kinematic model for evaluation of hemiparetic stroke. *Journal of Biomechanics* 2006; 39(4): 681-688.
26. Requejo PS, Wahl DP, Bontrager EL, Newsam CJ, Gronley JK, Mulroy SJ, et al. Upper extremity kinetics during lofstrand crutch-assisted gait. *Medical Engineering & Physics* 2005; 27(1): 19-29.
27. Zatsiorsky VM. Joint torques and forces: The inverse problem of dynamics. In: Robertson LD, ed. *Kinetics of human motion.* Vol 2. Champaign, IL: Human Kinetics; 2002: 365-454.
28. Slavens BA, Sturm PF, Harris GF. Upper extremity inverse dynamics model for crutch-assisted gait assessment. *Journal of Biomechanics* 2010; 43(10): 2026-2031.